Numerical and experimental study of a rotating magnetic particle chain in a viscous fluid

Y. Gao and M. A. Hulsen*
Department of Mechanical Engineering, Eindhoven University of Technology, Eindhoven, The Netherlands

T. G. Kang
School of Aerospace and Mechanical Engineering, Korea Aerospace University, Goyang-city, Republic of Korea

J. M. J. den Toonder
Department of Mechanical Engineering, Eindhoven University of Technology, Eindhoven, The Netherlands and Philips Corporate Technologies, Royal Philips Electronics, Eindhoven, The Netherlands

(Received 6 June 2012; revised manuscript received 7 September 2012; published 9 October 2012)

A simple and fast numerical method is developed capable of accurately determining the 3D rotational dynamics of a magnetic particle chain in an infinite fluid domain. The focus is to control the alternating breakup and reformation of the bead chain which we believe is essential to achieve effective fluid mixing at small scales. The numerical scheme makes use of magnetic dipole moments and extended forms of the Oseen-Burgers tensor to account for both the magnetic and hydrodynamic interactions between the particles. It is shown that the inclusion of hydrodynamic interaction between the particles is crucial to obtain a good description of the particle dynamics. Only a small error of deviation is observed when benchmarking the numerical scheme against a more computationally intensive method, the direct simulation method. The numerical results are compared with experiments and the simulated rotational dynamics correspond well with those obtained from video-microscopy experiments qualitatively and quantitatively. In addition, a dimensionless number (R_T) is derived as the sole control parameter for the rotational bead chain dynamics. Numerically and experimentally, $R_T \approx 1$ is the boundary between rigid "rod" and dynamic "breaking and reformation" behaviors.

DOI: 10.1103/PhysRevE.86.041503 PACS number(s): 83.10.Pp, 83.80.Gv, 45.50.−j, 47.11.−j

I. INTRODUCTION

The development of laboratory-on-chip systems that enable classical biochemical assays to be integrated and accomplished on one single chip [1] is currently a hot topic. When functionalized with biospecific surface coatings, magnetic particles can be used inside laboratory-on-chip systems for the selective capture and/or detection of the target molecules. Critical reviews dealing with various applications of magnetic particles in laboratory-on-chip systems, such as labeling, sorting, transporting, and mixing, are presented by Gijs *et al*. [2] and Pamme *et al*. [3].

In such systems, due to their small dimensions and low flow rates, the selective capture of a biomolecule is limited by diffusion [4]. It is believed that by controlled actuation of the suspended magnetic particles, the transport of the target molecules can be made chaotic, which will significantly enhance the capture efficiencies and shorten the detection time. Specifically, Suzuki *et al*. [5] showed that the probability of selective binding between the coated magnetic particles and the target biomolecules is maximized in the chaotic regime, which can be obtained through effective fluid mixing.

Many studies, both computational and experimental, have investigated the controlled actuation of suspended magnetic particles as well as its potential application to chaotically mix fluid streams at micro scale. In this study, we focus on the controlled rotational dynamics of a single magnetic particle chain in an infinite fluid domain. A diluted, monodispersed and uniformly distributed superparamagnetic colloidal suspension is exposed to a strong, continuous, homogenous, and unidirectional magnetic field. Under such circumstances, the suspended magnetic particles form isolated magnetic particle chains. When the magnetic field begins to rotate, the isolated chains also tend to rotate in order to remain oriented with the field.

Melle *et al*. [6–9] studied experimentally the global dynamics of multiple-interacting chainlike structures. They used the Mason number to define the observed dynamics. At low Mason numbers, the chainlike structures rotate with the magnetic field frequency. At higher Mason numbers, the induced structures breakup. For comparison, Melle *et al*. [7–9] conducted particle dynamics simulations. Despite neglecting the effect of hydrodynamic interaction between the particles, the simulations show good agreement with the experiments.

Rotational dynamics of isolated magnetic particle chains have also been studied extensively [10–13]. The rotating chains are observed to undergo a process of dynamic growth and fragmentation that is dependent on the frequency of the applied field. Typical structures such as linear chains and S-shaped chains are noted. Yadav *et al*. [12] and Krishnamurthy *et al*. [13] observed that the particle dynamics method is able to predict the macroscopic chain dynamics accurately. But, for microscopic properties, inclusion of hydrodynamic interactions becomes important.

Recently, Kang *et al*. [14] conducted 2D finite element simulations to solve the induced fluid flows actuated by a single rotating magnetic particle chain. They concluded that, within a limited range of the Mason numbers, periodic breaking and reformation of the magnetic particle chain occur. This repeating topological change of the chain is the most efficient way to induce mixing of fluids at the micro scale. Specifically,

*m.a.hulsen@tue.nl

the alternating breakup and reformation lead to the stretching and folding of fluid elements, which is a manifestation of chaos. Numerically and experimentally, Sing *et al*. [15] and Franke *et al*. [16] have also observed the alternating chain break and chain reformation at the chain center of a rotating magnetic particle chain, indicating the first chain breakup transition.

To the best of our knowledge, little attention has been given to the numerical and experimental comparisons of such alternating topological changes, indicating the critical control parameter. Moreover, although there is much previous work on modeling the dynamics of suspended magnetic particles, most of these studies employed either a simplified but fast simulation method (particle dynamics, pin-jointed mechanism) or a more detailed but computationally expensive method (Stokesian dynamics, lattice Boltzmann, and finite elements simulations). In the present study, we expand the fast 3D particle dynamics simulation with extended forms of the Oseen-Burgers tensor to account for the effect of hydrodynamic interactions. Similar numerical approaches, in some regards, have been reported by Sing *et al*. [15] and Vilfan *et al*. [17]. This numerical scheme is subsequently benchmarked against a more accurate but cumbersome simulation method (3D version of the numerical scheme developed by Kang *et al*. [18]). A 2D numerical approach using the Oseen-Burgers tensor was investigated by Cregg *et al*. [19]. In addition, we carried out video-microscopy experiments to obtain the repeating topological changes of the chain for qualitative and quantitative comparisons.

II. NUMERICAL METHODS

A complete theoretical analysis regarding the dynamics of suspended superparamagnetic particles in Newtonian fluids actuated by a homogeneous magnetic field involves various contributions. Here, we consider only those contributions which we believe are essential to capture the physics of the problem, i.e., the alternating breakup and reformation dynamics of an isolated rotating magnetic particle chain in an infinite fluid domain.

A. Magnetic interactions

Given the superparamagnetic nature of the particles, we can assume that their magnetization is always parallel to the applied field. Moreover, we expect that the strength and the direction of bead magnetization are not affected by neighboring magnetic particles. Thus, each magnetic particle is modeled as a hard sphere characterized by its induced magnetic dipole moment,

$$\mathbf{m} = V_p \chi_p \mathbf{H}, \tag{1}$$

where V_p is the spherical volume of the suspended particles, χ_p the effective magnetic particle susceptibility, and $\mathbf{H}$ the applied magnetic field. The spherical shape of the particles induces an internal demagnetization field opposite to the applied magnetic field, reducing the magnetic susceptibility of the particle relative to the magnetic susceptibility of the material of which it is composed. This phenomenon is included in the Clausius-Mossoti function for the calculation of the effective magnetic susceptibly for a spherical particle [20],

$$\chi_p = \frac{\chi}{1 + \frac{\chi}{3}}, \tag{2}$$

where χ is the magnetic susceptibility of the material of which the particle is composed. Since, in our simulations, the applied magnetic field is homogeneous, there is no magnetic gradient force due to the applied field. Thus, the expression for the magnetic interaction force $\mathbf{F}_i^m$ acting on the i^{th} superparamagnetic particle in a collection of N particles equals [9,13]

$$\mathbf{F}_i^m = \frac{3\mu_0}{4\pi} \sum_{\substack{j=1 \\ j \neq i}}^{N} \frac{m_i m_j}{r_{ij}^4} [(1 - 5(\hat{\mathbf{m}} \cdot \hat{\mathbf{r}}_{ij})^2)\hat{\mathbf{r}}_{ij} + 2(\hat{\mathbf{m}} \cdot \hat{\mathbf{r}}_{ij})\hat{\mathbf{m}}], \tag{3}$$

where μ_0 is the magnetic permeability of free space, m_i the strength of the dipole moment of the ith particle, $\hat{\mathbf{m}}$ is the unit vector of the magnetic field, r_{ij} is the distance between the centers of the ith and jth particles, and $\hat{\mathbf{r}}_{ij}$ the unit vector of the corresponding two-particle chain axis.

The excluded-volume force is implemented to model "hard" sphere particles and, thus, to prevent them from overlapping [9,13],

$$\mathbf{F}_i^{\text{ev}} = 2\frac{3\mu_0}{4\pi(2R)^4} \sum_{\substack{j=1 \\ j \neq i}}^{N} m_i m_j e^{-\xi(\frac{r_{ij}}{2R}-1)} \hat{\mathbf{r}}_{ij}, \tag{4}$$

where R is the particle radius. Here, numerical simulations are performed with $\xi = 30$. Using this value for ξ in a configuration where two dipoles aligned with the magnetic field are separated by a distance of $2.2R$, the corresponding excluded volume force acting on a single particle is 14 times smaller than the opposing magnetic attraction force. Thus, its influence on isolated dipoles is negligible.

B. Hydrodynamic interactions

The movement of a particle through the fluid will influence the corresponding flow field and, consequently, the motion of other particles. This hydrodynamic interaction between the particles is a complex phenomenon and involves many contributions, such as the nonlinear character of the Navier-Stokes equation for the fluid flow. We neglect inertia of the fluid and assume Stokes flow. In that case, a linear relationship exists between the force $\mathbf{F}(\mathbf{r}_j)$ exerted by the jth particle at position $\mathbf{r}_j$ on the fluid and the velocity perturbation of the flow field $\Delta\mathbf{v}(\mathbf{r}_i)$ at some other position $\mathbf{r}_i$. Here, the force exerted on the fluid by the jth particle is equal in magnitude but opposite in direction to the hydrodynamic drag force $\mathbf{F}_j^h$ experienced by the corresponding particle, i.e., $\mathbf{F}(\mathbf{r}_j) = -\mathbf{F}_j^h$. In view of the linear Stokes equation, it is natural to assume that the velocity perturbations caused by the different beads can be superimposed, i.e., the total velocity perturbation of the flow field at position $\mathbf{r}_i$ caused by $(N-1)$ particles equals [21]

$$\Delta\mathbf{v}(\mathbf{r}_i) = \sum_{\substack{j=1 \\ j \neq i}}^{N} \boldsymbol{\Omega}(\mathbf{r}_{ij}) \cdot \mathbf{F}(\mathbf{r}_j) \tag{5}$$

with $\mathbf{\Omega}(\mathbf{r}_{ij})$ known as the Oseen-Burgers tensor. However, in deriving the original form of the Oseen-Burgers tensor, the assumption of point particles with zero radius was made, which is certainly unjustified.

Several studies proposed the use of extended forms of the Oseen-Burgers tensor in which the influence of the finite size of the particles with radius R is approximately taken into account. The best known modification is the Rotne-Prager-Yamakawa tensor valid for interacting particles of equal size [22–24],

$$\mathbf{\Omega}(\mathbf{r}) = \frac{3}{24\pi\eta r}\begin{cases}\left[\left(1+\frac{2R^2}{3r^2}\right)\mathbf{I}+\left(1-\frac{2R^2}{r^2}\right)\frac{\mathbf{rr}}{r^2}\right], & r \geqslant 2R\\ \left[\frac{r}{2R}\left(\frac{8}{3}-\frac{3r}{4R}\right)\mathbf{I}+\frac{\mathbf{rr}}{8R^2}\right], & r < 2R\end{cases}, \tag{6}$$

where η is the dynamic viscosity of the nonmagnetic fluid and $\mathbf{I}$ the unit tensor. Öttinger [21,22] proposed a hydrodynamic-interaction tensor that smoothly switches off the interactions at short distances (of order R),

$$\mathbf{\Omega}(\mathbf{r}) = \frac{1}{8\pi\eta r\left[r^2+\left(\frac{4}{3}\right)R^2\right]^3}\left[\left(r^6+\frac{14}{3}R^2r^4+8R^4r^2\right)\mathbf{I} + \left(r^6+2R^2r^4-\frac{8}{3}R^4r^2\right)\frac{\mathbf{rr}}{r^2}\right]. \tag{7}$$

They argued that the above modification, due to its smooth dependence on the position vector, can be important for the systematic development of higher-order numerical integration schemes for the stochastic differential equations of motion. However, only the Rotne-Prager-Yamakawa tensor has been proven to be valid for all configurations of chains consisting of any number of beads [21]. In the current work, both hydrodynamic-interaction tensors are incorporated in the numerical model to compare their influences on the rotating bead chain dynamics.

Furthermore, if we assume that the hydrodynamic drag force acting on the ith particle equals the Stokes drag, the following relationship can be derived between the hydrodynamic drag force, the ith particle velocity $\mathbf{v}_i$, and the fluid velocity at the particle position $\mathbf{r}_i$, $\mathbf{v}(\mathbf{r}_i)$,

$$\mathbf{F}_i^h = -6\pi\eta R[\mathbf{v}_i - \mathbf{v}(\mathbf{r}_i)] \tag{8}$$

In general, there are three contributions to the fluid velocity $\mathbf{v}(\mathbf{r}_i)$: (a) the externally imposed fluid velocity field, (b) the motion driven by the forces exerted by the other particles in the system [see Eq. (5)], and (c) the correction to the velocity experienced by the particle due to the presence of confining walls [25]. In the simulation of suspended magnetic particles in an infinite medium, the fluid velocity at position $\mathbf{r}_i$ is due to contribution (b), i.e., $\mathbf{v}(\mathbf{r}_i) = \Delta\mathbf{v}(\mathbf{r}_i)$.

C. The numerical system

Ignoring the negligible inertia of the particles, the governing equation for the ith superparamagnetic particle is given by

$$\mathbf{F}_i^m + \mathbf{F}_i^{\text{ev}} + \mathbf{F}_i^h = 0, \tag{9}$$

where $\mathbf{F}_i^m$ is the magnetic force, $\mathbf{F}_i^{\text{ev}}$ the excluded-volume force, and $\mathbf{F}_i^h$ the hydrodynamic force. Melle *et al.* [7] defined a dimensionless number λ that calculates the ratio between magnetic and thermal energies,

$$\lambda = \frac{\pi\mu_0 R^3\chi_p^2 H_0^2}{9\kappa_B T}, \tag{10}$$

where H_0 is the magnitude of the magnetic field, κ_B the Boltzmann constant, and T the temperature. The values of λ that correspond to the conducted experiments reported here are between 1400 and 3800. Therefore, the magnetic force was the dominating force during the experiments and Brownian motion was, thus, neglected in the simulations. Since we are interested in the dynamic behavior of a rotating magnetic particle chain in an infinite fluid domain, chain sedimentation is of no importance. The corresponding numerical scheme can be found in Appendix A.

In this paper, a 3D particle dynamics model is developed that is capable of predicting the dynamic behavior of magnetic colloids in an infinite medium exposed to an externally applied magnetic field. While this method is simple, it includes the hydrodynamic interactions between the particles. In other words, the motion of a particle depends on the motion of the other particles. For comparison, we will also perform particle dynamics simulations where hydrodynamic interaction is neglected.

III. NUMERICAL BENCHMARKING

First, we benchmarked the obtained numerical model against a more accurate but computationally expensive method, the direct simulation method introduced by Kang *et al.* [18]. The direct simulation method uses the Maxwell stress tensor and a fictitious domain method to solve both magnetic and hydrodynamic interactions between the particles in a fully coupled manner. Both simulation methods are formulated in 3D.

The model problem (Fig. 1) involves two spherical magnetic particles (with radius R) suspended in a Newtonian fluid with negligible wall boundary effects. The initial distance between the two particle centers equals $4R$. The resulting particle-center trajectory is dependent on the initial phase lag α, formed between the direction of the magnetic field $\mathbf{H}$ and the axis of the bead chain.

The particles with radius $R = 1$ are modeled with a material magnetic susceptibility $\chi = 1$ which corresponds to an effective magnetic particle susceptibility $\chi_p = 0.75$. The particles are suspended in a Newtonian fluid with a dynamic viscosity $\eta = 0.001$ and are subjected to a static, homogenous

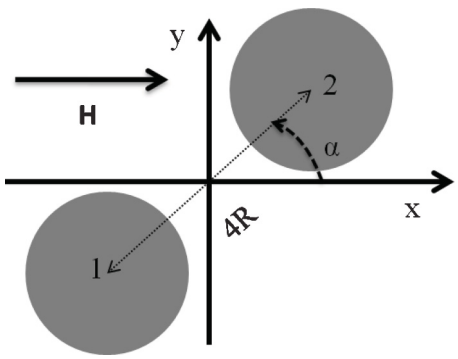

FIG. 1. The model problem used to benchmark particle dynamics simulation method against the direct simulation method.

magnetic field with a magnitude $H_0 = 1000$. Using the direct simulation method as a point of reference, two types of particle dynamics simulations are carried out to study the effect of hydrodynamic interaction between the particles. One includes the implementation of the hydrodynamic-interaction tensors, whereas in the other one hydrodynamic interaction is not considered. Discrete time steps $\Delta t = 10^{-6}$ are used for all the conducted simulations.

In Figs. 2(a)–2(c), particle-center trajectories as a function of the initial phase lags are plotted using particle dynamics simulations (symbols) and the direct simulation method (lines). The Rotne-Prager-Yamakawa tensor [Eq. (6), Fig. 2(a)] and the Öttinger tensor [Eq. (7), Fig. 2(b)] are used to approximate the effect of hydrodynamic interaction between the particles. The variation in initial phase lags is represented by a difference in symbols and colors. Regardless of the initial particle configuration ($\alpha < 90°$), the two particles eventually move towards each other, forming a chain aligned with the magnetic field. Apart from close interparticle distances, the simulated results correspond very well with each other. The deviation seen at the end of the trajectories is caused by the lubrication phenomenon, which is not included in the particle dynamics simulations.

On the other hand, if hydrodynamic interaction is not considered, significant deviations can be found between the particle dynamics simulation and the direct simulation method. In Fig. 2(c), it is seen that discrepancies exist even if the two particles are relatively far from each other ($\alpha = 80°$). Thus, we can conclude that inclusion of hydrodynamic interaction between the particles is crucial to accurately determine the trajectories of suspended magnetic particles. In addition, first-order approximations regarding the magnetic and hydrodynamic interactions between the particles are shown to yield similar results with respect to the simulation method in which hydrodynamic interactions and high-order mutual magnetic interactions are solved in a fully coupled manner.

In Fig. 2(d), the obtained particle-center trajectories are plotted as a function of time in a system configuration where

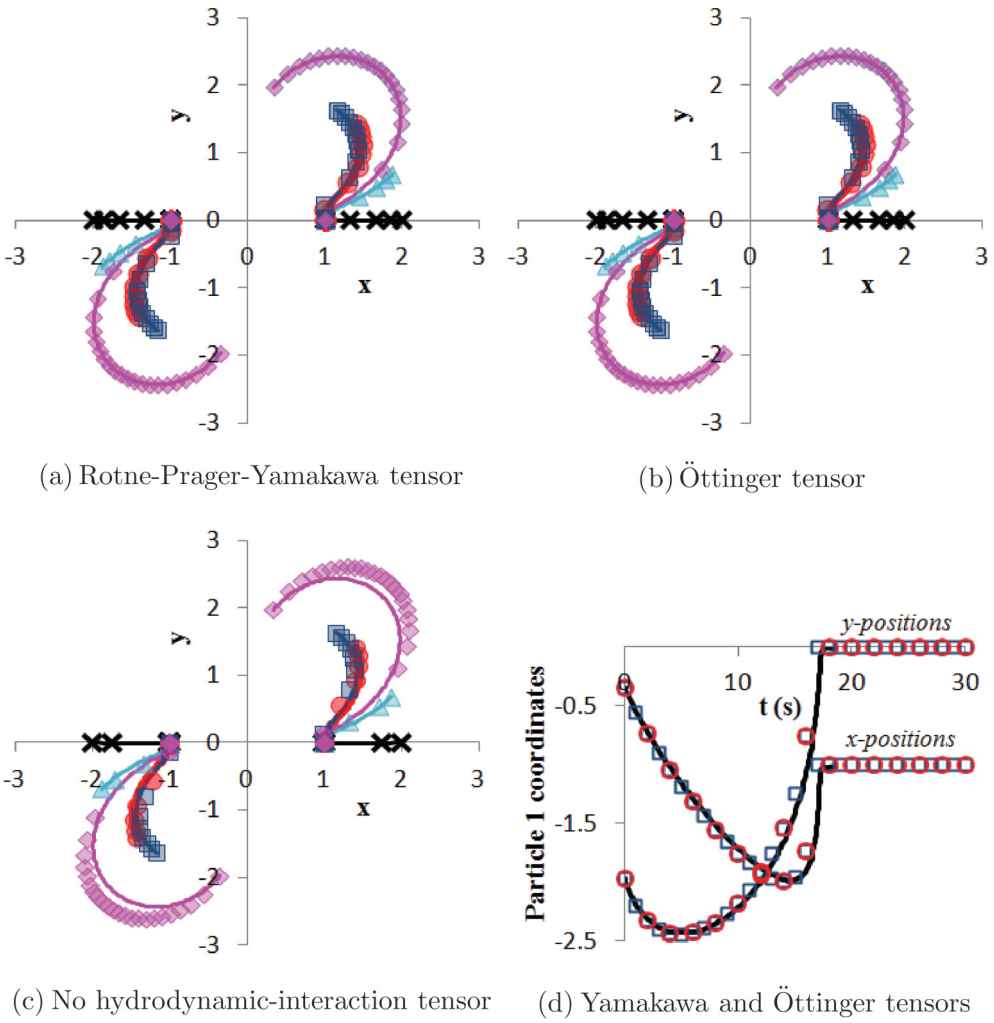

(a) Rotne-Prager-Yamakawa tensor (b) Öttinger tensor

(c) No hydrodynamic-interaction tensor (d) Yamakawa and Öttinger tensors

FIG. 2. (Color online) Benchmarking results between particle dynamics simulations (symbols) and the direct simulation method (lines). [(a)–(c)] Particle-center trajectories as function of the initial phase lags. The initial phase lags are 0° (black cross), 20° (cyan triangle), 45° (red circle), 54.7° (blue square), and, finally, 80° (magenta diamond). (d) Particle-center trajectories as function of time in which the initial phase lag equals 80°. The x and y coordinates of particle 1 are calculated using the Rotne-Prager-Yamakawa tensor (square) or the Öttinger tensor (circle).

the initial phase lag was 80°. Here, we follow the x and y coordinates of particle 1 (Fig. 1) calculated using either hydrodynamic-interaction tensors or the direct simulation method. A small deviation of 4.5% in the time scale can be seen between the two types of simulation methods. We believe that the cause is due to the first-order approximations made for both the magnetic and the hydrodynamic forces.

Summarizing, although the direct simulation method provides a more accurate description of the magnetic and hydrodynamic interactions between the particles, it is computationally expensive, cumbersome, and even practically unfeasible when calculating the three-dimensional dynamics of multiple particles ($N > 2$). In contrast, the 3D particle dynamics simulation method implemented with a hydrodynamic-interaction tensor has the capacity to simulate a large collection of suspended particles in a relatively short time. Moreover, first-order approximations cause a deviation error of only around 4.5%, which, we believe, is still small enough to give an accurate prediction of the suspended particle dynamics.

IV. EXPERIMENTAL METHODS

Experiments were carried out with diluted suspensions of superparamagnetic particles at room temperature ($T =$ 293 K). A magnetic actuation setup was realized capable of manipulating the magnetic particles triaxially, i.e., by generating a user-specified magnetic field both in the horizontal as well as in the vertical plane [Figs. 3(a) and 3(b)]. The setup consists of eight individually controlled coils (brown) together with eight soft-iron (ARMCO) poles (gray) connected by soft-iron frames (blue and red). Magnetic fields are produced by the flow of electrical currents through the coils and by following the soft-iron frames, and they are guided to the sample area as indicated by a cross sign at the center of the setup.

In the current study, we are interested in the biaxial actuation of the suspended magnetic particles and their subsequent breakup and reformation dynamics. Therefore, only the part of the setup (blue) capable of creating a horizontal rotating homogeneous magnetic field is of importance here. Using that part of the setup [Fig. 3(c)], a magnetic field was generated and was measured using a Gauss meter (F. W. Bell). Within the sample area (2 × 2 mm), the generated magnetic field is homogenous and has a linear relationship with the actuation current, i.e., electrical currents with amplitudes of 0.2 and 0.1 A produce constant magnetic fields of 13 (±0.4) and 6.5 (±0.3) mT, respectively.

The fluid chamber (which is placed in the center of the setup) has a diameter of 9 mm and a depth of 1 mm and is made using polystyrene substrates and Secure-Seal spacers (Grace BIO-LABS) [Fig. 3(d)]. The bead suspension was placed inside the fluid chamber, which was then closed with a cover glass. All experiments were conducted at a constant magnetic field strength while varying the frequency of the rotation. During each experiment, the setup was placed under a microscope (Leica) and the dynamics of induced bead chains were subsequently analyzed using video microscopy. Only free-floating bead chains were considered, i.e., bead chains without any interactions with each other and the surrounding walls of the reservoir.

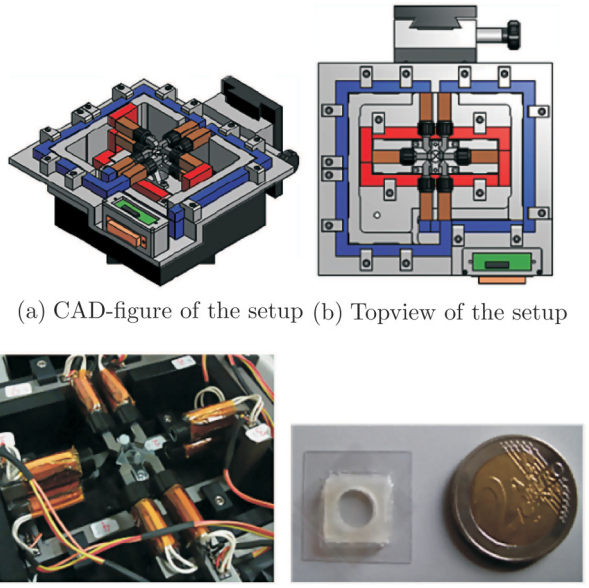

(a) CAD-figure of the setup (b) Topview of the setup

(c) Horizontal actuation configuration (d) The fluid chamber

FIG. 3. (Color online) Magnetic actuation setup and fluid chamber. [(a) and (b)] CAD figures of the setup. (c) The part of the setup capable of creating a horizontal rotating homogeneous magnetic field. (d) The fluid chamber that is placed in the center of the setup.

We chose to work with particles coated with carboxylic acid (COOH) groups to prevent particle aggregation and clogging and to obtain stable and repeatable bead chain dynamics. Two different polymer-based superparamagnetic particles were used in the experiments, i.e., Micromer particles (3 μm, Micromod) and M-270 Dynabeads (2.8 μm, Invitrogen). The magnetic properties of the particles were determined using vibrating sample magnetometer (VSM) measurements for both the Micromer particles ($\chi_p \approx 0.19$) as well as for the Dynabeads ($\chi_p \approx 0.69$) at the field strengths applied in the experiments.

V. A PARTICLE CHAIN MODEL

Three-dimensional particle dynamics simulations were carried out to determine the dynamic behavior of magnetic colloids under the influence of a rotating magnetic field. We are interested in the alternating breakup and reformation behavior of an isolated magnetic particle chain suspended in an infinite medium.

With reference to several authors [6,10,11,18,26,27], the integrity of a chain is determined by its phase lag, which is defined as the angle between the long axis of the chain and the externally applied magnetic field. When this phase lag increases above a critical number, the radial component of the dipolar magnetic force [Eq. (3)] responsible for chain formation becomes negative, causing the chain to fragment. This phase lag is due to competition between two opposing angular torques: a driven magnetic torque counteracted by a viscous drag torque. In the case when the viscous torque is larger than the maximum possible magnetic torque, the phase lag grows beyond its critical number and the chain subsequently fragments.

Generally, rotating magnetic particle chain dynamics have been characterized by the use of the Mason number [7,9–14, 26,28]. Although this dimensionless parameter is described using different proportionality factors in the literature, it is always defined as the ratio of hydrodynamic to magnetic forces for a two-particles-in-contact configuration. In contrast, the alternating breakup and reformation configuration is the result of two competing angular torques rather than forces and is significantly influenced by the amount of particles forming the chain. Thus, we have derived a new dimensionless number (Appendix B) to characterize this special region of interest,

$$R_T = 16\frac{\eta\omega}{\mu_0\chi_p^2 H_0^2}\frac{N^3}{(N-1)\left(\ln\left(\frac{N}{2}\right)+\frac{2.4}{N}\right)}, \qquad (11)$$

where ω is the angular velocity of the applied magnetic field and N the amount of particles forming the chain. R_T is obtained by dividing the viscous drag torque [11,27,29] by the driven magnetic torque [11]. Just prior to chain fragmentation, the viscous torque equals the maximum obtainable magnetic torque, so $R_T = 1$ and the chain rotates following the magnetic field.

This dimensionless number leads to the subdivision of the rotating chain dynamics into two global regimes in agreement with the ones proposed by Melle *et al.* [7,9] and Kang *et al.* [14]. If $R_T < 1$, the magnetic torque balances the viscous torque and a steady phase lag is achieved, i.e., the bead chain rotates as a rigid rod following the field. But, if R_T grows beyond unity, chain fragmentation occurs. Thus, we define a critical R_T, R_{Tc} at which a bead chain begins to fragment and reform and based on the simplified theory for deriving R_T (Appendix B), R_{Tc} should be equal to 1 for any sizes of the chain.

The proposed dimensionless number R_T is consistent with the findings by Sing *et al.* [15]. They characterized the fragmentation (chain breakup) transition to be dependent on the square of the magnetic field magnitude and, inversely, on the square of the total amount of particles making up the chain. In addition, Melle *et al.* [9] concluded from experiments that the dynamics of chain rotation does not depend on particle volume fraction in diluted suspensions, which justifies the role of R_T as the sole control parameter in our simulations and experiments.

The model reflects an infinite liquid medium with suspended superparamagnetic particles subjected to a biaxial rotating homogeneous magnetic field. The initial spatial configuration of the colloids is an arrangement where the particles form chains aligned with the field. The externally applied magnetic field is the only driving force to actuate the particles. Its strength is constant but its direction varies with a constant angular velocity. All the simulated parameters, e.g., particle dimensional and magnetic properties, magnetic field strength, and fluid medium viscosity, are comparable to the ones used in the experiments.

VI. RESULTS AND DISCUSSION

Qualitative and quantitative comparisons are made between 3D numerical and experimental results of rotating chains of magnetic particles in an infinite fluid medium. As a first step, we investigate qualitatively and quantitatively the first breakup transition of a rotating magnetic particle chain, i.e., we obtain the critical R_T, R_{Tc}, at which a bead chain begins to fragment and reform. As a second step, we examine the higher-order breakup transitions experienced by a rotating magnetic particle chain as its R_T is increased above 1. Since the importance of including hydrodynamic-interactions is already pointed out in Sec. III, all the following numerical results take the effect of hydrodynamic interactions into account, calculated using the Rotne-Prager-Yamakawa tensor [Eq. (6)].

A. The first breakup transition

In Fig. 4, experimental [Figs. 4(a), 4(c), and 4(e)] and numerical [Figs. 4(b), 4(d), and 4(f)] results are depicted for a 14-bead chain. The R_{Tc} for a 14-bead chain equals 1.13 ($\pm$0.1) experimentally and 0.92 numerically. By varying R_T, the bead chain either rotates as a rigid rod following the field or it periodically breaks and reforms at the chain center in stable and predictable manner.

At relatively small values of R_T ($R_T < R_{Tc}$), the rotating bead chain has a linear shape. As the dimensionless number approaches the critical number ($R_T \leqslant R_{Tc}$), the bead chain deforms to obtain a stable S-shape with its ends following the field (as indicated by the black arrows) more closely than the rest of the chain. This phenomenon has been extensively studied by Petousis *et al.* [11]. Finally, when $R_T \geqslant R_{Tc}$, the bead chain breaks up and reconnects in an alternate manner.

A peculiarity is the breaking and reformation of an uneven magnetic particle chain that cannot break at the center, as is the case with the 14-bead chain. In Fig. 5, measured [Figs. 5(a) and 5(c)] and simulated [Figs. 5(b) and 5(d)] results are depicted for a 13-bead chain at $R_T > R_{Tc}$. Experimentally, the critical R_T for a 13-bead chain equals 1.05 ($\pm$0.05) and, numerically, it equals 0.94. If the experiment is conducted under ideal conditions, i.e., the magnetic particles have identical magnetic and dimensional properties without any external disturbances, the forces acting on the center particle due to its left and

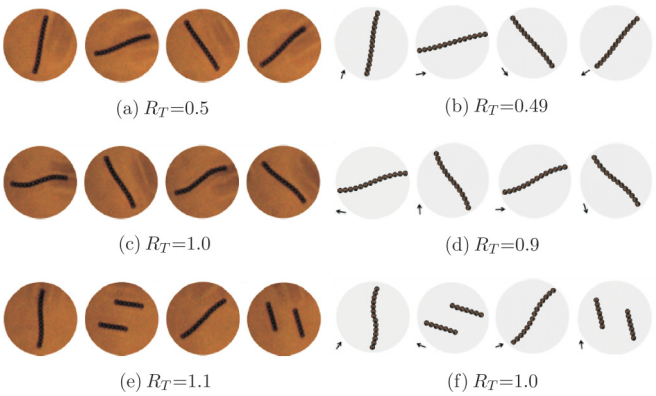

FIG. 4. (Color online) Rotational dynamics of a 14-bead (Dynabeads) chain characterized experimentally [(a), (c), and (e)] and numerically [(b), (d), and (f)]. By varying R_T, the bead chain either rotates as a rigid rod following the field or it periodically breaks and reforms at the chain center in stable and predictable manner. The black arrows indicate the directions of the magnetic field.

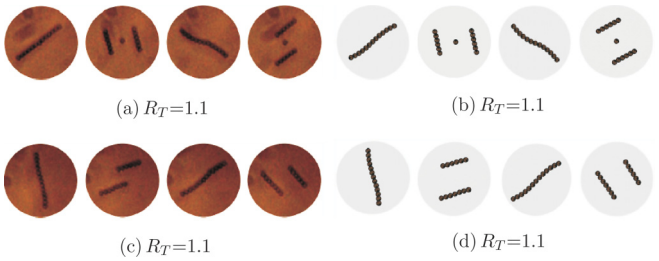

(a) R_T=1.1 (b) R_T=1.1

(c) R_T=1.1 (d) R_T=1.1

FIG. 5. (Color online) Breaking and reformation of a 13-bead (Dynabeads) chain studied experimentally [(a) and (c)] and numerically [(b) and (d)]. In (a) and (b), the observed dynamics occur only in ideal systems, whereas the dynamics in (c) and (d) correspond to systems with asymmetrical effects.

right neighbor bead chains have opposite directions and equal magnitudes and, hence, add to zero. The center particle therefore remains static while the outer bead chains tend to rotate [Fig. 5(a)].

This state of particle dynamics is very unstable: The experimental particles are not perfectly monodispersed nor do they have identical magnetic susceptibilities. Moreover, the particle surface interactions along with environmental disturbances such as the (small) nonhomogeneity of the applied magnetic field have to be taken into account. Thus, after two cycles of breaking and reformation, the symmetry of the system disappears and the bead chain quickly adapts to the behavior as depicted in Fig. 5(c).

Particle dynamics simulations were conducted under ideal conditions and the resulting configuration is a static particle in the center with two outer rotating bead chains [Fig. 5(b)]. In a next step, variability was incorporated in the simulation system by varying the magnetic properties of the particles [Fig. 5(d)]. Here, the magnetic susceptibility for each particle was randomly assigned from a uniform distribution in the interval [0.68, 0.7]. In this case, the bead chain breaks into two chains with an even and uneven amount of magnetic particles. For both systems, the obtained particle dynamics are very similar.

B. Quantitative comparisons of R_{Tc}

Quantitative comparisons between experiments and 3D particle dynamics simulations were obtained by observing the critical R_T for each rotating bead chain with length varying from 5 to 17 beads. In Fig. 6, the observed R_{Tc} is plotted as a function of the bead chain length. Experimentally, Micromer particles (due to their low magnetic susceptibility) form short bead chains (5–10 particles), whereas Dynabeads form relatively long bead chains (11–17 particles). Numerically [Fig. 6(a)], the effect of hydrodynamic interactions between particles is approximated using either the Rotne-Prager-Yamakawa tensor [Eq. (6)] or the Öttinger tensor [Eq. (7)]. For both hydrodynamic-interaction tensors, the obtained R_{Tc}'s (red square) are similar.

In addition, to emphasize the importance of implementing hydrodynamic-interaction tensors, numerical simulations [Fig. 6(b), purple diamond] were also conducted where Stokes drag was considered as the sole contribution to the hydrodynamic force acting on the particles, i.e., R_{Tc}'s were

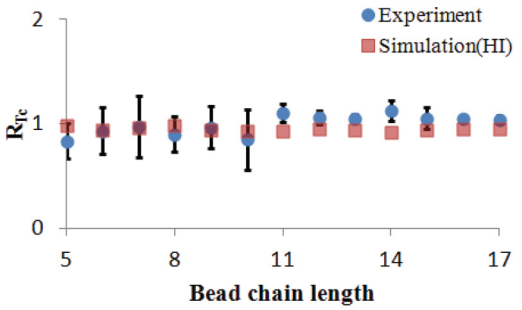

(a) Simulation vs. Experiments

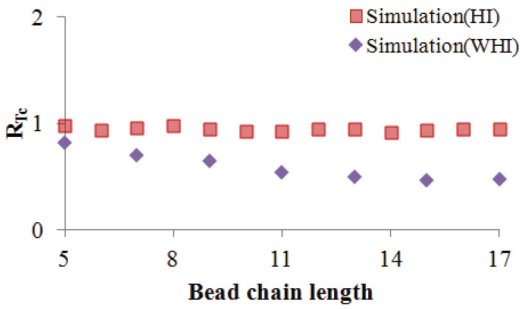

(b) Simulation vs. Simulation

FIG. 6. (Color online) In (a), quantitative comparisons are shown between numerical and experimental results of rotating bead chains at the point of fragmentation, characterized by the dimensionless number R_{Tc}. R_{Tc}'s of experimental bead chains are indicated by blue circles, whereas R_{Tc}'s of simulated bead chains are indicated by red squares. Here, the effect of hydrodynamic interactions is approximated using the Rotne-Prager-Yamakawa tensor [Eq. (6)]. In (b) simulations are conducted where the effect of hydrodynamic interactions is not considered (purple diamond).

obtained for simulated bead chains where hydrodynamic interaction between the particles was neglected.

In Fig. 6(a), it is seen that for both experiments and simulations, $R_{Tc} \approx 1$ is the boundary between rigid and dynamic behaviors, as we anticipated. Without the effect of hydrodynamic interactions [Fig. 6(b), purple diamond], R_{Tc} decreases from 0.8 for short chains to a value around 0.5 for long chains. This confirms the importance of including hydrodynamic interaction between the suspended magnetic particles.

In order to accurately determine the dynamics of the proposed particle chain model, one must take into account that the motion of a particle is dependent on the motion of other particles. We believe that the standard deviations [Fig. 6(a)] of the measurements are caused by the variations in the magnetic properties of the experimental microparticles. Nevertheless, we can conclude that, for both the experiments and the simulations, the critical R_T is around 1 and is independent of the chain length and taking the variations of the experiments into account, the numerical predictions are close to the experimental results. Thus, R_T seems to be an appropriate dimensionless number to characterize the rotational dynamics of a magnetic particle chain.

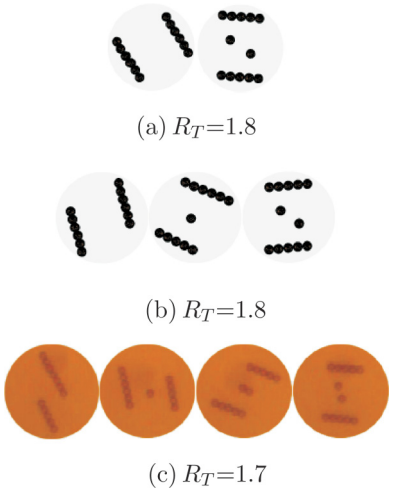

FIG. 7. (Color online) Dynamic behavior of a rotating 12-bead (Dynabeads) chain at the second breakup transition, studied numerically [(a) and (b)] and experimentally (c). The depicted topological changes are in sequence of the amount of chain fragments. Under assumption of identical magnetic properties (a), the 12-bead chain breaks alternately into two or four chain fragments. By varying the magnetic properties of the particles (b), asymmetric breakups occur. Movies corresponding to the rotational dynamics can be found in Supplemental Material [30].

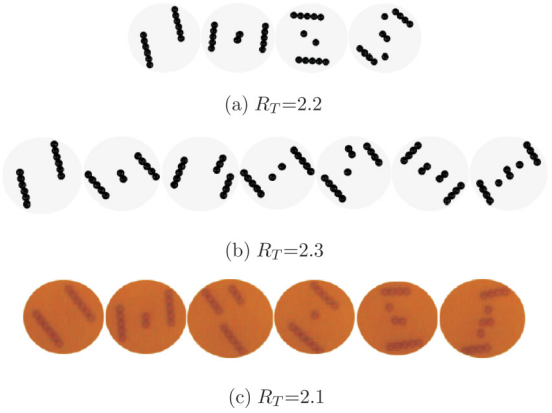

FIG. 8. (Color online) Dynamic behavior of a rotating 12-bead (Dynabeads) chain at the third breakup transition, studied numerically [(a) and (b)] and experimentally (c). Under assumption of identical magnetic properties (a), the 12-bead chain breaks into two, three, four, and five fragments. By varying the magnetic properties of the particles (b), asymmetric breakups occur. Movies corresponding to the rotational dynamics can be found in Supplemental Material [30].

C. The higher-order breakup transitions

For increasing R_T, we observed higher-order transitions at which additional chain dynamics appear with chains breaking into multiple pieces. Such higher-order breakup transitions of rotating magnetic particle chains were investigated both numerically and experimentally. In Fig. 7, rotational dynamics corresponding to the second breakup transition are shown for a 12-bead chain. The topological changes are depicted in sequence of the amount of chain fragments. Numerical simulations were conducted for both (1) the ideal case [Fig. 7(a)], i.e., the situation where the magnetic particles have identical magnetic properties and (2) the case where asymmetry was incorporated into the simulation system by varying the magnetic properties of the particles from a uniform distribution in the interval [0.68, 0.7] [Fig. 7(b)].

In Fig. 7(a), at $R_T = 1.8$, the 12-bead chain begins to breakup alternately into two or four chain fragments. Since particle dynamics simulations were conducted under ideal conditions, the resulting rotational dynamics of the magnetic particle chain is expected to be symmetric, which is indeed the case. In contrast, by varying the magnetic properties of the particles [Fig. 7(b)], a bead exists at the chain center with the lowest susceptibility and it is eventually released as the magnetic particle chain breaks into three fragments. When the chain center is occupied by magnetic particles with similar magnetic properties, the chain fragments into four pieces. Petousis *et al.* [11] suggested a bead of lower susceptibility to act as the weakest link. Such dynamic behavior, the alternating chain breakup and chain reformation with two, three, or four chain fragments, was also observed experimentally [Fig. 7(c)]. In real-life experiments, we also have to consider that both magnetic as well as dimensional variations along with particle surface interactions and environmental disturbances (small nonhomogeneity of the magnetic field) have additional effects on the rotational dynamics of the magnetic particle chains and they, consequently, account for the observed differences between experiments and simulations.

At even higher R_T, a third (Fig. 8) transition region was observed. Similarly as above, Fig. 8(a) corresponds to numerical simulations conducted under ideal conditions and Fig. 8(b) corresponds to ones conducted with varying magnetic particle properties. In the ideal case [Fig. 8(a)], in accordance with the above, the 12-bead chain symmetrically breaks up in two, three, four, and five chain fragments. Again, by varying the magnetic properties of the particles [Fig. 8(b)], asymmetric breakups occur which are indeed more similar to the obtained experimental results [Fig. 8(c)]. In Supplemental Material [30], movies corresponding to the rotational dynamics of a 12-bead chain can be found for both experiments and simulations.

Sing *et al.* [15] characterized the higher breakup transitions using numerical modeling and tracking the time-average number of chain fragments ($\langle n \rangle$) at an increasing dimensionless number, i.e., $\sim \omega N^2 H_0^{-2}$ which scales with R_T. They concluded that a master curve exists between the time-averaged number of chain fragments and the dimensionless number. It is interesting to see whether this can be confirmed by our experiments. In Fig. 9, the time-averaged number of chain fragments, with chain size varying from 9 to 14 beads, is plotted with respect to R_T. Here, the external magnetic field is kept constant at 5 and 9 mT while the chain length and field rotational frequency are varied. In accordance with the findings of Sing *et al.*, the data collapse to a master curve at different field strengths, different chain lengths, and different rotational frequencies.

The results obtained from experiments and simulations agree very well. More importantly, we found that the

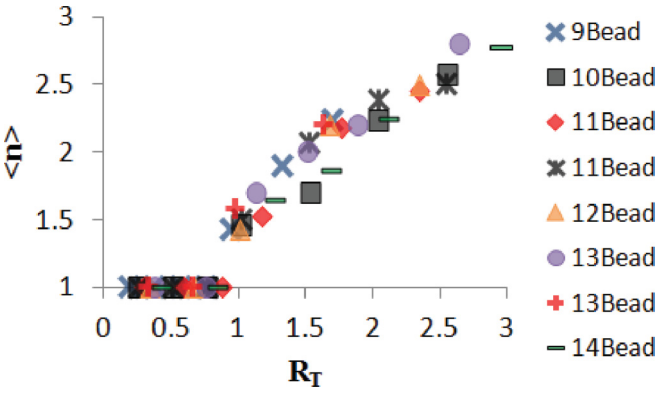

FIG. 9. (Color online) The time-average number of chain fragments with respect to R_T. The external magnetic field is kept constant at 5 mT (square, diamond, triangle, circle, rectangular) and 9 mT (crosses). The experimental rotating chains were varied from $N = 9$ to $N = 14$.

inclusion of asymmetric effects by varying the magnetic particle properties is crucial to obtain a good description of the particle dynamics at higher breakup transitions. Although the dimensionless number R_T is derived for the first breakup transition, i.e., the case when the viscous torque is larger than the maximum possible magnetic torque ($R_T > 1$), we believe that R_T can also be used to indicate the thresholds for higher-order breakup transitions.

VII. CONCLUSION

In the current work, we proposed a fast, easy-to-implement numerical method to accurately describe the dynamics of a rotating magnetic particle chain in an infinite fluid domain.

The numerical method, implemented using dipolar magnetic interactions and hydrodynamic-interaction tensors, was shown to yield a small error of 4.5% when benchmarked against the direct simulation method. Inclusion of hydrodynamic-interaction tensors was crucial to obtain such a small error of deviation. Although the direct simulation method provides a more accurate description of the magnetic and hydrodynamic interactions between the particles, it is practically unfeasible when calculating the 3D dynamics of multiple particles. In contrast, 3D particle dynamics simulations have the capacity to simulate a large collection of suspended particles in a relatively short time.

We derived a dimensionless number R_T that is capable of characterizing the dynamics of a rotating magnetic particle chain, i.e., if R_T is smaller than a critical number R_{Tc}, the chain rotates as a rigid rod following the field. But, if R_T grows beyond R_{Tc}, the chain periodically fragments and reforms. According to basic theoretic considerations, R_{Tc} should be equal to 1. Numerically and experimentally, $R_{Tc} \approx 1$ was indeed found as the boundary between rigid and dynamic behaviors. In addition, in accordance with the numerical findings of Sing *et al.* [15], a master curve is found to exist between experimental chain fragmentation behavior and the proposed dimensionless number R_T. Thus, we can conclude from both the experiments and simulations that R_T is a dimensionless number that can be used to characterize the rotational dynamics of a magnetic particle chain.

Qualitatively, the numerical and experimental results agree very well, i.e., the simulated rotational dynamics of a magnetic particle chain correspond well with those obtained from video-microscopy experiments. Quantitatively, the numerical scheme incorporated with the effect of hydrodynamic interactions is able to determine accurately the transitional behavior of a rotating bead chain. In addition, variability effects were incorporated into the numerical work to approach real-life experiments. In particular, varying the magnetic particle properties statistically between beads in a simulation is found to be crucial to obtain rotational dynamics at higher breakup transitions.

Concluding, the combination of a fast 3D numerical method along with a new dimensionless number and our experimental setup allows us to experimentally control a rotating magnetic particle chain and design the optimum parameters for real laboratory-on-chip applications. In the end, this can be utilized to effectively mix fluids and effectively capture low concentrations of biomolecules.

ACKNOWLEDGMENTS

The VSM measurements were carried out by Peter Graat of Philips Innovation Services. We acknowledge the members of the group Molecular Biosensors for Medical Diagnostics (TU Eindhoven) for their help in the experimental work. Similar thanks go to the engineers at GTD (TU Eindhoven) for manufacturing the setup. This work was supported by Technology Foundation STW under Grant No. 10458.

APPENDIX A: THE NUMERICAL SCHEME

The numerical scheme used to calculate ith superparamagnetic particle trajectory is as follows. As a first step, the hydrodynamic drag force acting on the ith particle is obtained from Eq. (9),

$$\mathbf{F}_i^h = -\left(\mathbf{F}_i^m + \mathbf{F}_i^{\mathrm{ev}}\right). \tag{A1}$$

As a second step, we obtain the net velocity of the ith superparamagnetic particle with respect to the surrounding fluid from Eq. (8),

$$\mathbf{v}_i - \mathbf{v}(\mathbf{r}_i) = -\frac{\mathbf{F}_i^h}{6\pi\eta R}. \tag{A2}$$

As a third step, the total velocity perturbation of the flow field surrounding the particle is calculated using $\mathbf{F}(\mathbf{r}_j) = -\mathbf{F}_j^h$ and Eqs. (5) and (A1),

$$\mathbf{v}(\mathbf{r}_i) = \sum_{\substack{j=1 \\ j\neq i}}^{N} \mathbf{\Omega}(\mathbf{r}_{ij}) \cdot \left(\mathbf{F}_j^m + \mathbf{F}_j^{\mathrm{ev}}\right). \tag{A3}$$

From Eq. (A2), the particle velocity $\mathbf{v}_i$ is obtained. As a last step, discrete time steps Δt are used to obtain the ith particle

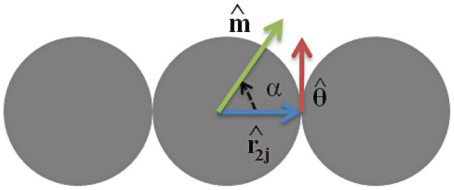

FIG. 10. (Color online) A three-bead chain.

trajectory using the following equation:

$$\mathbf{r}_i = \mathbf{r}_i + \mathbf{v}_i \Delta t, \tag{A4}$$

which is a forward Euler method.

APPENDIX B: DERIVATION OF R_T

The motion of a rotating magnetic particle chain is due to the tangential components of the dipolar magnetic interaction force [Eq. (3)]. Moreover, the corresponding magnetic force has an inverse dependence on particle center-center distance to the power 4. It is, therefore, justified to consider only nearest-neighbor dipole interactions for the calculation of the driving magnetic torque acting on a rotating magnetic particle chain. Assuming the suspended magnetic colloids to be identical both magnetically as well as dimensionally, the expression for the tangential component of the magnetic force $\mathbf{F}_2^{\theta}$, acting on the second superparamagnetic particle in a collection of three particles forming a rigid and straight chain is

$$\mathbf{F}_2^{\theta} = \frac{3\mu_0 m^2}{4\pi(2R)^4} \sum_{\substack{j=1 \\ j\neq 2}}^{3} [2\sin(\alpha)(\hat{\mathbf{m}} \cdot \hat{\mathbf{r}}_{2j})\hat{\theta}], \tag{B1}$$

where $\hat{\theta}$ is the unit vector perpendicular to the corresponding particle chain axis. In Fig. 10, a three-bead chain is depicted along with some of the parameters in Eq. (B1). The dot product term causes the tangential forces acting on a bead due to its left and right neighbors to have opposite directions and, hence, the total tangential force acting on the particle equals zero. Only for the outer particles that have just one direct neighbor is the net tangential force nonzero.

3D particle dynamics simulations with hydrodynamic-interaction tensors were conducted to validate the above assumption, i.e., only the outer particles of a chain have significant contributions to the driven magnetic torque. In Fig. 11(a), torque contribution (i.e., the cross product between the tangential force component acting on the particle and the position vector between the center of the chain and the center of the corresponding particle) of each particle in a 5-bead chain is plotted against time steps. Torque contributions of the outer particles are depicted by blue squares, whereas the rest of the particles are represented by black lines. A similar action is done for a 17-bead chain [Fig. 11(b)]. Again, torque contributions of the outer particles are depicted by the blue squares. For both figures, it is seen that beads with two neighboring particles have a negligible influence on the driven magnetic torque. Thus, we can conclude that the driven magnetic torque is determined by the tangential forces acting on the outer particles of a chain. Using the above statements, the driven magnetic torque is derived for an N-bead chain [11],

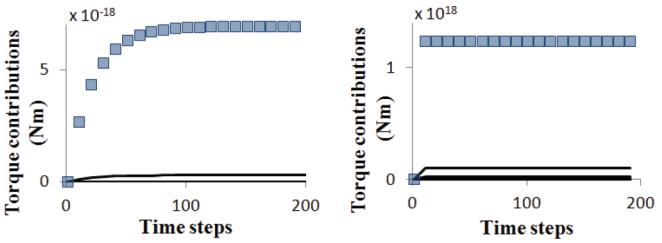

(a) 5-bead chain (b) 17-bead chain

FIG. 11. (Color online) Torque contributions of the particles forming a chain are plotted against time steps. Torque contributions of the outer beads are depicted by blue squares, whereas the rest of the particles are represented by black lines.

$$T_m = \frac{3\mu_0 m^2 (N-1)}{4\pi(2R)^3} \sin(2\alpha). \tag{B2}$$

The maximum possible torque occurs when the chain follows the rotating magnetic field with a constant phase lag of 45°.

The opposing viscous drag torque consists of four factors [11,27,29]. The first factor is the shape factor κ for a linear chain of spherical particles, including the effect of hydrodynamic interactions. Specifically, Wilhelm *et al.* [29] empirically derived a shape factor valid for any size of the chain,

$$\kappa = \frac{2N^2}{\ln\left(\frac{N}{2}\right) + \frac{2.4}{N}}. \tag{B3}$$

The second and third factors are the rotating chain volume and fluid viscosity, respectively. The fourth factor deals with the angular velocity of the rotating chain and equals the angular velocity of the rotating field when chain breaking did not occur. Combining the mentioned factors, the viscous drag torque equals

$$T_v = \frac{8\pi R^3}{3} \frac{N^3}{\ln\left(\frac{N}{2}\right) + \frac{2.4}{N}} \eta\omega. \tag{B4}$$

Just prior to chain fragmentation, the phase lag equals 45° and the chain rotates following the magnetic field. R_T [Eq. (11)] is obtained by dividing the viscous drag torque T_v by the driven magnetic torque T_m.

[1] P. Mitchell, Nat. Biotechnol. **19**, 717 (2001).
[2] M. A. M. Gijs, Microfluid. Nanofluid. **1**, 22 (2004).
[3] N. Pamme, Lab. Chip. **6**, 24 (2006).
[4] T. M. Squires and S. R. Quake, Rev. Mod. Phys. **77**, 977 (2005).
[5] H. Suzuki, H. Chih-Ming, and N. Kasagi, J. Microelectromech. Syst. **13**, 779 (2004).
[6] S. Melle, G. G. Fuller, and M. A. Rubio, Phys. Rev. E **61**, 4111 (2000).

[7] S. Melle, O. G. Calderón, G. G. Fuller, and M. A. Rubio, J. Colloid Interface Sci. **247**, 200 (2002).
[8] S. Melle, O. G. Calderón, M. A. Rubio, and G. G. Fuller, J. Non-Newtonian Fluid Mech. **102**, 135 (2002).
[9] S. Melle, O. G. Calderón, M. A. Rubio, and G. G. Fuller, Phys. Rev. E **68**, 041503 (2003).
[10] S. Melle and J. E. Martin, J. Chem. Phys. **118**, 9875 (2003).
[11] I. Petousis, E. Homburg, R. Derks, and A. Dietzel, Lab Chip **7**, 1746 (2007).
[12] A. Yadav, R. Calhoun, P. Phelan, A. K. Vuppu, A. A. Garcia, and M. Hayes, IEE Proc. Nanobiotechnol. **153**, 145 (2006).
[13] S. Krishnamurthy, A. Yadav, P. Phelan, R. Calhoun, A. Vuppu, A. Garcia, and M. Hayes, Microfluid. Nanofluid. **5**, 33 (2008).
[14] T. G. Kang, M. A. Hulsen, P. D. Anderson, J. M. J. den Toonder, and H. E. H. Meijer, Phys. Rev. E **76**, 066303 (2007).
[15] C. E. Sing, L. Schmid, M. F. Schneider, T. Franke, and A. Alexander-Katz, Proc. Natl. Acad. Sci. USA **107**, 535 (2010).
[16] T. Franke, L. Schmid, D. A. Weitz, and A. Wixforth, Lab Chip **9**, 2831 (2009).
[17] M. Vilfan, A. Potočnik, B. Kavčič, N. Osterman, I. Poberaj, A. Vilfan, and D. Babič, Proc. Natl. Acad. Sci. USA **107**, 1844 (2010).
[18] T. G. Kang, M. A. Hulsen, J. M. J. den Toonder, P. D. Anderson, and H. E. H. Meijer, J. Comput. Phys. **227**, 4441 (2008).
[19] P. J. Cregg, K. Murphy, A. Mardinoglu, and A. Prina-Mello, J. Magn. Magn. Mater. **322**, 2087 (2010).
[20] T. B. Jones, *Electromechanics of Particles* (Cambridge University Press, Cambridge, UK, 1995).
[21] H. C. Öttinger, *Stochastic Processes in Polymeric Fluids* (Springer, Berlin, 1996).
[22] W. Zylka and H. C. Öttinger, J. Chem. Phys. **90**, 474 (1989).
[23] B. Carrasco and J. G. de la Torre, Biophys. J. **76**, 3044 (1999).
[24] T. Geyer and U. Winter, J. Chem. Phys. **130**, 114905 (2009).
[25] M. D. Graham, Annu. Rev. Fluid Mech. **43**, 273 (2011).
[26] T. Roy, A. Sinha, S. Chakraborty, R. Ganguly, and I. K. Puri, Phys. Fluids **21**, 027101 (2009).
[27] S. L. Biswal and A. P. Gast, Phys. Rev. E **69**, 041406 (2004).
[28] S. L. Biswal and A. P. Gast, Anal. Chem. **76**, 6448 (2004).
[29] C. Wilhelm, J. Browaeys, A. Ponton, and J. C. Bacri, Phys. Rev. E **67**, 011504 (2003).
[30] See Supplemental Material at http://link.aps.org/supplemental/10.1103/PhysRevE.86.041503 for movies of rotational dynamics of simulated and experimental 12-bead chains.